Effects of neutron irradiation and post-irradiation annealing on pop-in crack propagation instabilities in 6061 aluminium alloy

Tom Petit, Claire Ritter, Jacques Besson, Thilo F. Morgeneyer

Neutron irradiation and heat treatment effects on pop-in crack propagation instabilities in a 6061 aluminium alloy

Tom Petit[1,*], Claire Ritter[1], Jacques Besson[2], Thilo F. Morgeneyer[2]

[1] Université Paris-Saclay, CEA, DES - Service d'Etude des Matériaux Irradiés, 91191, Gif-sur-Yvette, France
[2] MINES ParisTech, PSL Research University, Centre des matériaux, CNRS UMR 7633, France

Abstract

This study analyses the increase of crack propagations instabilities (pop-in) with irradiation during fracture toughness testing of an aluminium alloy 6061 alloy after neutron irradiation. The aim is to identify if the crack propagation instabilities are related to microstructural heterogeneities, i.e. weak zones, or if they are linked to a competition between testing machine stiffness and tearing modulus.

A mechanical analysis is performed comparing the testing machine stiffness to the tearing moduli of the irradiated materials. For this purpose an experimental program is carried out in the hot cells facility at CEA Saclay to conduct mechanical and microstructural studies, after irradiation in a Material Testing Reactor (mean conventional thermal fluence: $6.8.10^{21}$ $n_{th.conv}.cm^{-2}$).

The material hardening is quantified in this study using tensile tests after the heat treatments. The effect of this hardening on crack propagation instabilities is measured by fracture toughness tests on irradiated and precracked CT12.5 samples. Damage mechanisms are studied by SEM fractography and classical ductile fracture micromechanisms are found for all conditions without notable differences between non irradiated and irradiated materials. The evolution of toughness with irradiation and subsequent heat treatments is therefore attributed to the matrix hardening/softening and its effect on nucleation of voids on brittle second phase particles as evidenced by the same authors for classical age hardening of the alloy.

To investigate experimentally if the crack propagation instabilities are related to the tearing moduli, heat treatments of the irradiated material are applied that soften the material. It is shown that with softening, the number of crack propagation instabilities decreases and eventually the pop-ins disappear. The instability criteria using J-Δa R-curves of the toughness tests are applied and it is concluded that the increase in pop-ins with irradiation is resulting from the decrease of the material tearing modulus (and its interaction with the machine stiffness).

The toughness test results of the irradiated material of the present study are compared with those of the literature and show very good agreement.

Keyword: Irradiation effects, aluminium, fracture mechanisms, hardening, toughness

Highlights

- Mechanical tests are performed after heat treatments on irradiated 6061 aluminium
- Matrix hardening due to irradiation causes the decrease of toughness properties
- Crack instabilities are due to the decrease of the tearing modulus
- Fractography shows typically ductile fracture mechanisms after irradiation
- These mechanisms are identical in any state: irradiated or not, heat-treated or not

* Corresponding author
E-mail address: tom.petit@cea.fr (T. Petit)

1. Introduction

1.1. Neutron irradiation effects

The 6061-T6 material is used as structural material of the pressure vessel in research nuclear reactors. It is thus exposed to high neutron flux. The locations in the centre of reactors are exposed to irradiations presenting a high amount of fast neutrons ($E > 0.1\ MeV$), whilst the outer regions are exposed to a mixed spectrum having a high thermal flux ($E = 0.025\ eV$) in the reflecting materials for the experiments on nuclear fuel.

The T6 state is achieved by thermal treatment leading to a fine and homogeneous precipitation of *β''* nanoprecipitates [2,3], leading to its maximum hardening [4]. In the materials' microstructure there are also Cr and Mn rich dispersoid particles having a size in the order of hundreds of nanometers. In addition, there are micrometer sized second phase particles (iron rich impurities and Mg_2Si particles). During irradiation the 6061-T6 will undergo microstructural changes due to both contributions of the irradiation spectrum [5–9].

1.1.1. Effects of fast neutron flux (E>0.1 MeV)

First, neutron irradiation causes ballistic radiation damage: the fast flux causes phase transformation (second phase dissolution) and displacements of atoms in cascades , thereby creating interstitials, vacancy defects, dislocations and voids [5–9]. These damages due to fast neutrons could also have a direct impact on the phases, in particular the nanometer-sized *β''*, but authors in the literature are not unanimous concerning the stability of these phases under irradiation:

- Farrell and King [8] did not observe modifications of these phases after a fast fluence of 18.10^{22} n/cm² (thermal fluence of 30.10^{22} n/cm²).
- In contrast, Weeks et al. [9] found that *β''* dissolved accompanied by the formation of a new spherical phase at a fast flux of 2.10^{22} n/cm² (thermal fluence of 42.10^{22} n/cm²). More recently, Flament et al. [10] observed the complete dissolution of the pre-existing *β''* precipitates and the formation of a new phase, caused by an *in situ* irradiation of Al^{2+} ions.

In addition to this ballistic damage, hydrogen and helium are formed and finally gather into gas bubbles that have been observed at grain boundaries [11]. By model irradiations using tungsten ions, Ribis et al. [12] showed the nucleation of a high density of small cavities. The thereby created defects harden the material and make it less ductile. This hardening effect is caused by the hampering of dislocation movement due to an increased amount of obstacles.

1.1.2. Effects of thermal flux (E=0.025 eV)

Secondly, the thermal flux causes the formation of Si-rich precipitates. This phenomenon is due to the transmutation of Al into Si (more precisely the transmutation of ^{27}Al into ^{28}Al which by β^- disintegration, transforms into ^{28}Si) [13,14]:

$$Al^{27}(n,\gamma) \rightarrow Al^{28} \rightarrow Si^{28} + \beta^-$$

This transmutation makes more Si available in solid solution which favours, in combined action of the fast flux, the formation of *β''* and *β'* as long as Mg is available. Farrell [15] showed that the phase that appeared in AA5052-O was finer than the one typically formed in a classical treatment of 6061 alloys. These precipitates also harden the material due to their coherence with the matrix. Farrell [16] showed that this precipitation is accompanied by an increase in strength (in terms of yield and ultimate tensile strengths) and a decrease in ductility (quantified by uniform and total plastic elongations) for an alloy 5052-O. When there is no Mg available the created Si form precipitates whose structure is amorphous and

incoherent with the matrix. Under strong flux, it could precipitate on grain boundaries and thereby reduce the fracture toughness of 6061 [9] and 5052-O [16]. It should be noted that once the solubility limit of Si in the Al matrix is reached, Si atoms can also precipitate in form of spherical nanophases, that also contribute to a volume increase (called swelling) of the material [5,8,9].

According to the works of Farrell [17], the thermal flux plays the major role compared to the fast flux in terms of precipitate evolution during irradiation. It should also be noted that the micrometer-sized precipitates are not affected by irradiation [18].

An original study is presented in Appendix A, where a formula is proposed to calculate the rate of silicon transmuted as a function of thermal fluence.

1.1.3. Mechanical properties after irradiation

There are only few published research works concerning the effects of the microstructural evolution on mechanical properties. Concerning tensile properties, Farrell and King showed in different studies [5,7,8] an increased strength (increase in yield strength and UTS by a factor of 1.5 to 1.65 as a function of irradiation parameters) and a substantial loss of ductility (in terms of elongation). According to Kapusta et al [19], this loss of ductility is quantified by a reduction in total elongation; this reduction is related to the content of silicon generated under neutron flux, while strength is little affected by the high amount of silicon production. Farrell and King also found a transition from a transgranular to an intergranular ductile fracture mechanism, which is confirmed by Munitz et al. [20] who found that radiation hardening of 6063 aluminium alloy is accompanied by a transition from transgranular shear fracture to intergranular fracture.

Weeks and Czajkowski also confirmed for 6061-T6 this hardening [21] (which they attribute mainly to the thermal flux rather than to the fast flux, and therefore to the transmutation of silicon), accompanied by a significant loss of toughness [9] at room temperature (Figure 1). However, Albertin [22] noted that, compared to the evolution of tensile properties, the toughness is little affected by irradiation. Similarly, Alexander [6,23] studied the crack growth resistance: it was characterized both by fracture initiation toughness (by determining the K_j value) and resistance to crack extension in term of tearing modulus (by determining the *dJ/da* value). He noted that the resistance to crack initiation of a 6061-T651 alloy is degraded in tests at 150 °C and appears to be little affected at 26 and 95 °C, despite a strength increase at these three temperatures (Figure 1). However, even if the material in the unirradiated state already has a very low crack propagation resistance, in terms of tearing modulus, Alexander noted a clear deterioration of the latter with irradiation at all three temperatures, resulting in an almost flat R-curve. The author correlated this evolution to the decrease in elongation at tensile failure with irradiation.

In addition, these studies by Alexander showed that the majority of tests showed one or more pop-ins (a phenomenon he refers to as "crack jump"). A pop-in is a rapid but limited crack propagation associated with a sudden decrease in load observed during some fracture toughness tests. There are more pop-ins in the irradiated state: at a temperature of 26 °C (respectively 95 and 150 °C), tests with an average of 2 (resp. 3 and 2.3) pop-ins in the unirradiated state evolve to tests with an average of 4.3 (resp. 4 and 5.5) pop-ins after irradiation at a fluence of 10^{22} $n_{th}.cm^{-2}$. Finally, Alexander pointed out that the use of a power law to adjust R-curve is not suited when pop-ins exist. Indeed, the concave shape induced by such an adjustment can lead to a negative tearing modulus, which is physically absurd.

As part of a CEA (The French Alternative Energies and Atomic Energy Commission) research project, several toughness tests were carried out on 6061-T6 specimens irradiated with different fluences in CEA Saclay's OSIRIS research reactor. In particular, they were carried out on four castings that differ slightly in their chemical composition, their forming route and the applied heat treatments. 184 toughness tests

were analysed to quantify the number of tests with at least one pop-in as a function of irradiation (more precisely as a function of conventional thermal fluence, expressed in $n_{th}.cm^{-2}$ for a neutrons' energy of 0.025 eV). Figure 2 illustrates the result of this statistical study.

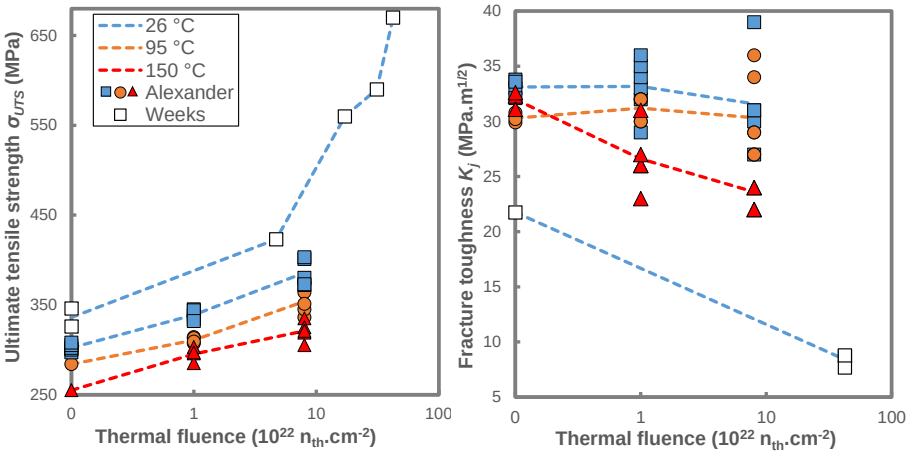

Figure 1 - Evolution of ultimate tensile strength σ_{UTS} and fracture toughness K_J in function of thermal conventional fluence for three test temperatures. Graphs using Alexander's [6,23] and Weeks' [9] data, respectively with a thermal/fast neutron fluence ratio of 2 and 21.

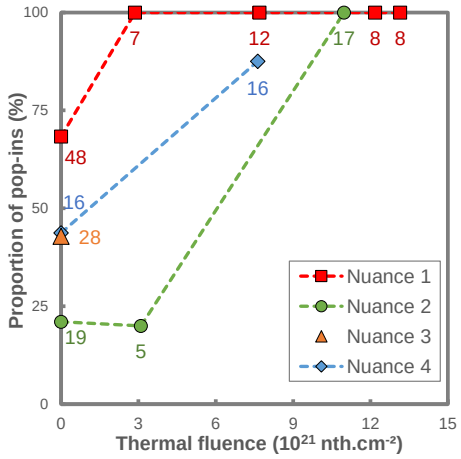

Figure 2 – Fraction of toughness tests with at least one pop-in, as a function of conventional thermal fluence, for four 6061-T6 aluminium castings (184 tests analysed – the numbers correspond to the number of specimens tested for each condition)

The fraction of tests with pop-in clearly increases with irradiation, reaching 100 % of tests that have showed at least one pop-in. One of the objectives of this study is therefore to understand this phenomenon. To investigate this phenomenon and understand its cause, two related studies are needed:

- First, it is necessary to consider the influence of irradiation on mechanical properties (in particular on mechanical strength and tearing modulus) and damage mechanisms.
- Second, it is necessary to determine whether the pop-ins observed in the irradiated state have the same mechanical origin as those observed in the unirradiated state, namely the interaction identified by Petit et al. [1] between the material tearing modulus and the stiffness of the test machine. This interaction has been proven:
  - experimentally using a dedicated device to reduce the machine stiffness.

- analytically through the formulation of instability criteria (see part 4). Figure 3 schematizes one of the instability criteria: a pop-in is triggered when the additive inverse of the machine stiffness equals to the local slope of $P(u_s)$ curve (P is the load, u_s is the load-line displacement).
- numerically by finite element modelling of this interaction between the specimen and the test machine [24].

It had also been shown that these purely mechanical pop-ins occurred only during the crack propagation regime (decreasing load), and not during the crack initiation regime (increasing load).

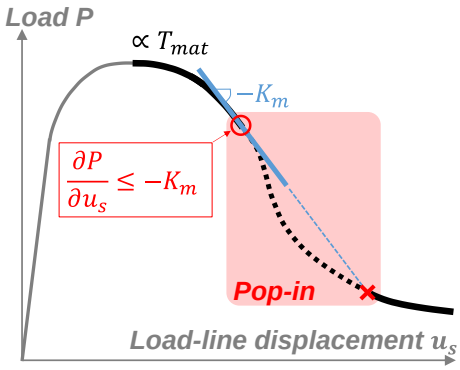

Figure 3 - Schematic showing graphical instability criterion to pop-in initiation and arrest [1]

1.2. Approach/structure of the paper

In the unirradiated state, the present authors have shown that pop-ins are related to an interaction between the stiffness of the testing machine and a decrease in the resistance to crack propagation, quantifiable by determining the tearing modulus [1]. We have also shown [25] that this decrease is not related to a change in damage mechanisms or to a modification of the coarse intermetallic particles, but is only the result of matrix hardening by nano-precipitation (observed by the atom probe tomography). By means of simulations integrating damage and in particular damage nucleation depending on stress, the key role of this hardening was highlighted [25].

Indeed, as described in the previous sections, the literature shows that irradiation has two effects on 6061 aluminium in particular:

- Firstly a hardening of the alloy [5–9,16,19,20,23].
- Second, a decrease in toughness [6,9,23], which is accompanied by an increase in the number of pop-ins [6,23].

According to the studies presented in [1,25,24], it can be assumed that these two effects are probably actually correlated: perhaps it might be the radiation-induced hardening, in analogy to structural hardening induced by aging, which causes the decrease in resistance to crack propagation, which, in turn, favours the appearance of pop-ins.

Thus, the strategy of the present work consists in choosing a material that shows a lot of pop-ins in the irradiated state, and in trying to soften the material by a suitable heat treatment. The objective is to determine whether this softening is accompanied by a disappearance of pop-ins. The constraints and precautions necessary for the handling of irradiated materials being numerous, the experimental campaign is therefore ambitious, as it involves several steps:

- Irradiation in the research reactor OSIRIS at CEA Saclay in order to sufficiently damage the material and change the material properties.
- Adapted heat treatments to soften the material, trying to create intermediate metallurgical states.

- Tensile tests to quantify this softening.
- Toughness tests to quantify the resistance to crack propagation and the pop-ins.
- Scanning Electron Microscope (SEM) fractographs to characterize damage mechanisms.

The application of the same instability criteria as those established for unirradiated material [1] will make it possible to determine the type of observed pop-ins. This study will also make it possible to compare the results obtained in the irradiated state with those obtained in the unirradiated state.

2. Methods

2.1. Material

The material used in this study (grade 1 in Figure 2) is an aluminium alloy 6061 (Al-Mg-Si), as received in a T6 condition. After a homogenization, the metal was shaped by a hot forging process to a ferrule form, then it underwent a solution annealing (at 532 °C during 4 hours), a water quenching and an isothermal age-hardening heat treatment at 175 °C during 8 hours. The chemical composition is given in Table 1. As explained in part 1.1, during irradiation the thermal flux causes the transmutation of Al into Si. A new method for calculating the transmutation rate is described in Appendix A. It can be seen that the chemical composition of an initially unirradiated 6061 alloy can exceed the range of validity of mass concentrations during irradiation; indeed, using the initial chemical composition of the material in this study, the higher mass concentration limit of Si (0.8 %) is reached at 6.2 10^{21} $n_{th.conv}.cm^{-2}$, and the lower mass concentration limit of Al (95.8 %) is reached at 64.5 10^{21} $n_{th.conv}.cm^{-2}$. At the fluence studied here (6.8 10^{21} $n_{th.conv}.cm^{-2}$), the Si concentration (0.81 %) has just exceeded the higher limit.

Si	Mg	Fe	Cr	Cu	Mn	Zn	Ti	Al
0.65	1.01	0.24	0.18	0.30	0.09	0.20	0.02	bal.

Table 1 – Initial chemical composition (mass percentage) of the studied 6061-T6 alloy

Previous studies performed by the CEA Saclay indicate that at least one pop-in was observed on all fracture toughness tests performed on irradiated samples (whereas in the unirradiated state, only 70 % of the samples exhibited at least one pop-in).

Tensile specimens are smooth round bars (gage length of 26 mm, diameter of 4 mm), fracture toughness specimen are notched standard Compact Tension (CT) samples (thickness $B_0 = 12.5\,mm$, net thickness $B_N = 10\,mm$, width $W = 25\,mm$). Tensile specimen were machined from this material on the circumferential (C) direction and fracture toughness specimen on the circumferential – radial (CR) direction (loading direction parallel to the circumferential direction and propagation of the crack parallel to the radial direction). More explanations concerning the geometries are detailed in [1]. All mechanical tests were performed at room temperature and under standard atmosphere, in both unirradiated and irradiated states.

2.2. Irradiation conditions

The samples to be irradiated were introduced in the research nuclear reactor OSIRIS of the CEA Saclay, between 2010 and 2013. They were arranged and maintained in experimental rigs (baskets), in sample holders in aluminium alloy. Once introduced in its water box, the device was directly immersed in water in the periphery of the reactor. The cooling is carried out through water thermal forced convection, the water circulating around and through the sample holder. The temperature in the sample holder, the baskets and the samples, is calculated, accounting for both volume heat production by gamma heating and heat extraction due to convection. The integrated thermal and fast fluence were measured and calculated a posteriori through the counting of dose integrators (niobium, iron, copper, or co-rolled aluminium-cobalt wires) introduced in canisters fixed on the baskets: the AlCo dosimeters allow to estimate thermal

conventional fluences and flux ($E = 0.025\ eV$), the Nb and Fe dosimeters allow to estimate fast fluences and flux ($E > 1\ MeV$).

The chosen conditions for irradiation were as close as possible to the flux conditions encountered in the research reactors in operation, both in terms of thermal neutrons flux and spectrum index: the highest thermal neutron flux is obtained at the first periphery of the heart of OSIRIS, where the ratio thermal flux / fast flux is around 10. This ratio is satisfying because it is increasing the embrittlement effects under irradiation in comparison with a ratio around 2 obtained in the OSIRIS core. In the chosen location for the samples of this study, the ratio was about 8 at the maximum flux plane. In order to homogenize the flux of the samples, rotations of 180° of the sample holder were performed at each irradiation intercycle. The irradiation conditions in the OSIRIS basin for this experience were the following:

- Environment: water.
- Irradiation temperature in the heart of the samples: 30 to 40 °C depending of the sample type (generally the most compact samples, like fracture toughness samples, are the warmest).
- Conventional thermal flux corrected at the maximum flux plane: $2.43.10^{14}$ n.cm^{-2}.s^{-1}.
- Fast flux at the maximum flux plane: $2.95.10^{13}$ n.cm^{-2}.s^{-1} at the middle of a basket.

The irradiated tensile and fracture toughness samples underwent respectively 18 and 20 cycles, which corresponds to a mean conventional thermal fluence of about $6.8.10^{21}$ $n_{th.conv}$.cm^{-2}. The thermal fluences experienced by each sample are given in Table 2. The baskets were afterwards unpacked in the LECI hot cells facility.

		Thermal fluence		Sample number	HT		
					Time	Temp.	
		10^{21} $n_{th.conv}$/cm^2			h	°C	
Tensile tests		Unirradiated		251	No HT (as received, T6)		
				252			
		7.52	7.50	222	No HT (as received, T6)		
			7.45	223			
			7.52	225			
		6.18	6.19	245	12	175	
			6.15	246	24		
			6.31	249	3	250	
			6.21	248	3	300	
			6.15	247	3	415	
Fracture toughness tests	**With partial unloading**	Unirradiated		J17-1	No HT (as received, T6)		
				J17-2			
				J17-3			
	Monotonic	6.70	6.91	159	No HT (as received, T6)		**+SEM**
			6.72	165	12	175	
			6.67	161	24		
			6.63	169	3	250	
			6.87	167	3	300	**+SEM**
			6.89	163	3	415	

Table 2 - Irradiation fluences and heat treatments applied to samples to study the irradiation effect. +SEM indicates the samples observed at the SEM in part 3.3.

2.3. Mechanical testing and heat treatments

All machining, mechanical testing and SEM observations of the samples were performed at the LECI hot cells facility (Figure 4), a laboratory dedicated mostly to the characterization of irradiated materials; it belongs to the Section of Research on Irradiated Materials (Nuclear Material Department) of the CEA Saclay, France.

2.3.1. Precrack

CT12.5 specimens were precracked on a hydraulic tension / compression machine INSTRON 8800 equipped with a 25 kN load cell in fatigue at room temperature ($f = 5\ Hz$, $\Delta K = 7\ to\ 5\ MPa\sqrt{m}$, $\frac{K_{min}}{K_{max}} = 0.25$, $C_g = -0.134$ [1]). Crack extension was monitored using the unloading compliance technique with an extensometer measuring the Crack Mouth Opening Displacement (CMOD) along the load-line of the sample. Depending on the specimen, more than 75000 up to 105000 cycles were necessary for the crack to reach a targeted a_0/W ratio of 0.6 (precrack length $a_0 \approx 15\ mm$).

Figure 4 - Photo of the LECI hot cells facility

2.3.2. Heat treatments

In order to soften the irradiated material, several heat treatments (HT) were performed in an oven OV 1738. For each heat treatment, one tensile and one fracture toughness sample were introduced in the oven with a reference sample instrumented with a thermocouple in order to control the temperature inside the oven. The temperature rise lasted for 30 to 60 min according to the target temperature, which was then maintained during a precise duration. The oven was then turned off and opened to cool the samples, with about 10 °C/min cooling rates. From the lightest to the most severe in terms of effects on mechanical properties, the heat treatments were the followings: no HT (as received, T6), 12 h at 175 °C, 24 h at 175 °C, 3 h at 250 °C, 3 h at 300 °C, 3 h at 415 °C (Table 2).

2.3.3. Mechanical tests

Tensile tests were performed on an INSTRON 8862 electromechanical static tensile machine equipped with a 50 kN load cell, using a strain rate of $10^{-4}\ s^{-1}$.

Fracture toughness tests were performed monotically (without unloading/reloading sequences) on the same machine used for the precracking, at room temperature. A crosshead displacement speed of 0.15

[1] $C_g = \frac{\ln(\Delta K_{final} - \Delta K_{initial})}{a_{final} - a_{initial}}$

mm/min was applied (corresponding roughly to 0.16 mm/min of CMOD speed). An EL 7/11/-160 LESCATE extensometer with blades, mounted across the mouth of the notch, records the samples CMOD. The samples were afterwards fatigue post-cracked, then observed at a macroscope, where initial fatigue crack length and stable crack growth were measured through nine-point measurements, in order to determinate the actuel initial and final advance of the crack.

The corresponding *J* values were computed according to ASTM 1820 [26]. Fracture toughness tests are analysed using the same procedure as in [1], using the numerical keycurve method to determine the crack length during the test. The keycurve method consists in (i) generating Load-Displacement curves for different fixed initial crack lengths a_0 using 3D elasto-plastic finite element simulations, (ii) determining the intersection of each simulated curve with the experimental one thereby indicating the current crack length at the intersection point.

2.3.4. Scanning Electron Microscopy (SEM)

In order to compare the damage mechanisms between the unirradiated and irradiated states and between two samples with or without pop-in, two Compact tension (CT) tested half (broken) samples were chosen to be analysed by scanning electron microscope (SEM) fractographs: from the N°159 sample (no heat treatment (as received, T6), with pop-in) and from the N°167 sample (3 h at 300 °C, no pop-in). Each half sample underwent several ethanol cleanings with ultrasound and was dried. Dose rates were measured to be: 37.1 mSv/h for the half N°159 sample, 45.1 mSv/h for the half N°167 sample.

The analyses were performed on a ZEISS SUPRA 55 microscope. The FEG (Field Emission Gun) SEM is equipped with several detectors: secondary electrons, backscattered electrons with four quadrants and "intra column" in lens detectors. Three analyses systems were supplied by the Oxford society: EDS (Energy Dispersive X-ray Spectroscopy) to identify precipitates, WDS (Wavelength Dispersive Spectroscopy) and EBSD (Electron Backscatter Diffraction) for grain distribution investigation. The nuclearization of the SEM allows studying samples up to a 500 mSv/h dose rate. For the two samples of this study, the observation conditions were the followings: secondary electrons detector, 10 kV acceleration tension, 60 µm diaphragm, 8 mm working distance.

3. Results

3.1. Tensile tests

The ten tensile test results are shown in Figure 5. Using these experimental data a Voce hardening law [27] is fitted for each aging time:

$$\sigma = \sigma_S + (\sigma_e - \sigma_S)e^{-b\varepsilon_p} \qquad \text{Eq. 1}$$

where σ_e is the yield stress, σ_S is the Voce saturation stress and b the Voce constant. These parameters are fitted using the tensile test results up to the onset of necking. The identified set of parameters is shown in Table 3 and is used in the 'keycurve' method [1] to construct the '*J-Δa*' curves. The results obtained after the treatments at 175 °C (12 and 24 h) being very close, they will be averaged in the rest of this paper. Without subsequent HT, the irradiation causes the hardening of the aluminium alloy. As expected, the gradually intensified HT after irradiation causes a gradual softening of the irradiated material (Table 3).

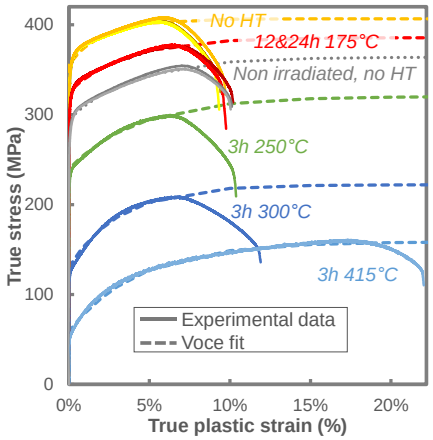

Figure 5 - Experimental tensile curves and fitted curves (Voce law) for unirradiated (gray curves, as received T6) and irradiated specimens (the other curves, with or without HT after irradiation); it should be noted that stress values after maximum load do not correspond to the true stress and are only given for indication of ductility

		σ_e MPa	σ_S MPa	b	σ_{UTS} MPa	σ_{UTS}/σ_e	A_g %	A %
Unirradiated	**No HT, as received (T6)**	295	364	25.4	330	1.12	6.6	10.7
		356	407	48.2	380	1.07	4.9	9.8
Irradiated	**12&24 h, 175 °C**	325	386	29.0	353	1.09	5.6	9.7
	3 h, 250 °C	240	320	23.1	280	1.17	5.8	10.8
	3 h, 300 °C	130	222	31.2	194	1.49	6.5	12.5
	3 h, 415 °C	59	159	23.1	135	2.29	16.2	23.6

Table 3 - Voce parameters and materials characteristics (A_g and A are respectively the uniform and total elongation, σ_{UTS} the ultimate tensile strength) obtained by tensile tests

3.2. Fracture toughness tests

Results are shown in Figure 6. As the three unirradiated tests with unloading showed superimposed results, only one test is presented in order not to overload the figure.

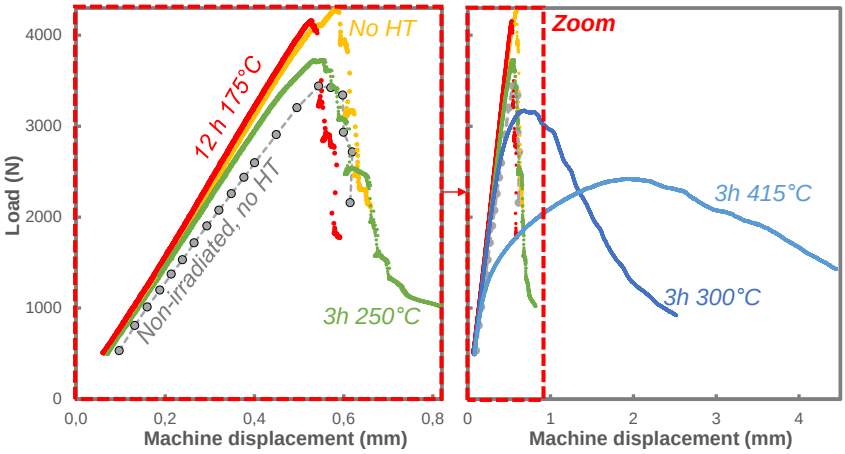

Figure 6 – Toughness test curves: load as a function of CMOD for unirradiated (gray curve, without HT) and irradiated specimens (the other curves, with or without HT). The figure on the left is a zoom of the figure on the right, without the 2 blue curves corresponding to the most severe heat treatments.

Two types of behaviour are observed, especially with regard to pop-ins (Table 4). The first behaviour is very close to the unirradiated state and concerns specimens not having undergone any HT or those having undergone a HT of 12 or 24 h at 175 °C, or of 3 h at 250 °C. For these metallurgical states, the load rises up to high values for a small machine displacement, then drops rapidly after the maximum. In that case, the CT samples show many pop-ins. The second behaviour concerns specimens that have been treated for 3 hours at 300 or 415 °C after irradiation: the load is lower and the slope's absolute value (*dF/dCMOD*) after the maximum is much smaller and the pop-ins disappear.

	Unirradiated			**Irradiated**					
	No HT			**No HT**	**175 °C**		**250 °C**	**300 °C**	**415 °C**
					12 h	**24 h**	**3 h**		
Number of pop-ins	2	3	3	3*	3	2	4	0*	0

Table 4 – Number of pop-ins for each fracture toughness test (: specimens observed at SEM)*

Note that it is easily observed, especially after the treatment at 250 °C, that the pop-ins occur systematically for decreasing force (as demonstrated analytically in [1]) in the crack propagation regime, even in the irradiated state.

3.3. Fractographic examination

Two fractured CT specimens were observed by SEM: the first one came from specimen 159 (no HT (T6, as received), three successive pop-ins), the second from specimen 167 (3 hours at 300 °C, no pop- in). Figure 7 compares the representative areas of each fracture surface at the same magnification.

The two top snapshots each result from the juxtaposition of sixteen snapshots taken at higher magnification. They make it possible to have a precise vision of the overall appearance of the fracture surface, and to determine the initial (end of the pre-cracking zone) and final (beginning of the fatigue post-cracking zone) advances of the crack, by averaging each time twenty measurements made over the entire width of the specimens. It can be seen that these advances are almost identical for both test specimens, which makes their comparison all the more interesting.

The fractographic examination show typical ductile fracture surfaces. Dimples are observed over the entire fracture surface for both specimens. Two characteristic lengths can be evidenced: mainly large dimples with a characteristic diameter of 10 to 20 μm (in the zones with void coalescence by internal necking), and some regions where the dimples are smaller with a characteristic diameter of 1 μm. These regions certainly correspond to shear zones with coalescence by void sheeting on a second population of smaller precipitates (dispersoids for example), as described in [28,29] for the unirradiated state.

Particles are found at the bottom of almost all of the coarse dimples. In the opposite case, it is very likely that these particles are located in the bottom of the dimple located in the second half-specimen. SEM-EDX analyses were performed on a few particles (see Appendix B), demonstrating that the majority are coarse Mg_2Si particles and some of them are Iron-rich Intermetallics (noted IM). Almost all of these particles are broken and have many cracks.

Concerning the fracture mechanisms, it is therefore important to emphasize that for the two studied specimens:

- The rupture is typically ductile, which results in the presence of many dimples on all fracture surfaces.

- The main nucleation mechanism is the fracture by cleavage (or fragmentation) of the Mg_2Si precipitates, rather than by inclusion/matrix decohesion. It was shown in [25,30] that nucleation on IMs occurs at higher levels of plastic strain.
- It should be noted that the coarse particles appear more fragmented in the irradiated state, which might be linked to the higher stress levels for the irradiated material. In the model for ductile fracture proposed in [25], the coarse Mg_2Si precipitates were considered as pre-existing voids/cracks because they fail in the very early loading stage [30]. In addition, the embrittlement of IMs due to irradiation could lead to an acceleration of the nucleation; in other words, cavities could nucleate at lower loading stages on these brittle phases.
- The growth and coalescence are affected by internal necking mainly (with dimples of about 10-20 μm in diameter) and by void-sheeting on some shear zones (with dimples of about 1 μm in diameter). No obvious evidence of intergranular failure was found.

In the case of irradiated materials, it can be seen that there is no difference in fracture surfaces between the two differently heat treated specimens, whether or not pop-ins have occurred. Pop-ins cannot be associated with a change in the nature of the fracture surface. In all cases the fracture surfaces are similar. This result is in agreement with observations made in the unirradiated state in [22], where pop-ins are also not identifiable on the fracture surface. Damage mechanisms do not seem to be significantly altered by irradiation at this scale.

4. Instability criteria analysis

It is therefore found that the irradiation causes the hardening of the material, which is accompanied by an increase in the number of pop-ins. With an increasingly intense HT after irradiation, a gradual softening of the material is found as well as a disappearance of pop-ins. As in the unirradiated state, the analysis of the damage mechanisms in irradiated materials evidences no difference between materials leading to pop-ins or not. In addition, there is no evidence of specific features on the fracture surface that could trigger pop-ins. This suggests that the type of pop-in occurring on the irradiated 6061 is an acceleration of ductile crack propagation, and that they do not result from a modification of the fracture mechanisms. In order to ensure that it is indeed this type of pop-in even in the irradiated state, it is necessary to apply the instability criteria proposed in [1]. The two tests corresponding to the specimens analysed by SEM, namely the specimens 159 (no HT, three successive pop-ins) and 167 (3 hours at 300 °C, no pop-in), were chosen.

The J-Δa curves, calculated by the keycurve method developed in [1] using the load-opening curves, are superimposed in Figure 8 (top). The irradiated material (yellow curve) exhibits larger J values than the unirradiated material (gray curve), which seems to reflect a slight beneficial effect of irradiation on fracture initiation toughness. The lower curves in Figure 8 are obtained by normalizing the J-integral with the flow stress σ_Y (mean of yield stress σ_e and ultimate tensile strength σ_{UTS}). With this normalization, it can be seen that both curves (unirradiated and irradiated material) are in agreement. This means that the slight increase in apparent toughness with irradiation is only due to the hardening (about 50 MPa), which does not seem to deteriorate the intrinsic toughness of the material.

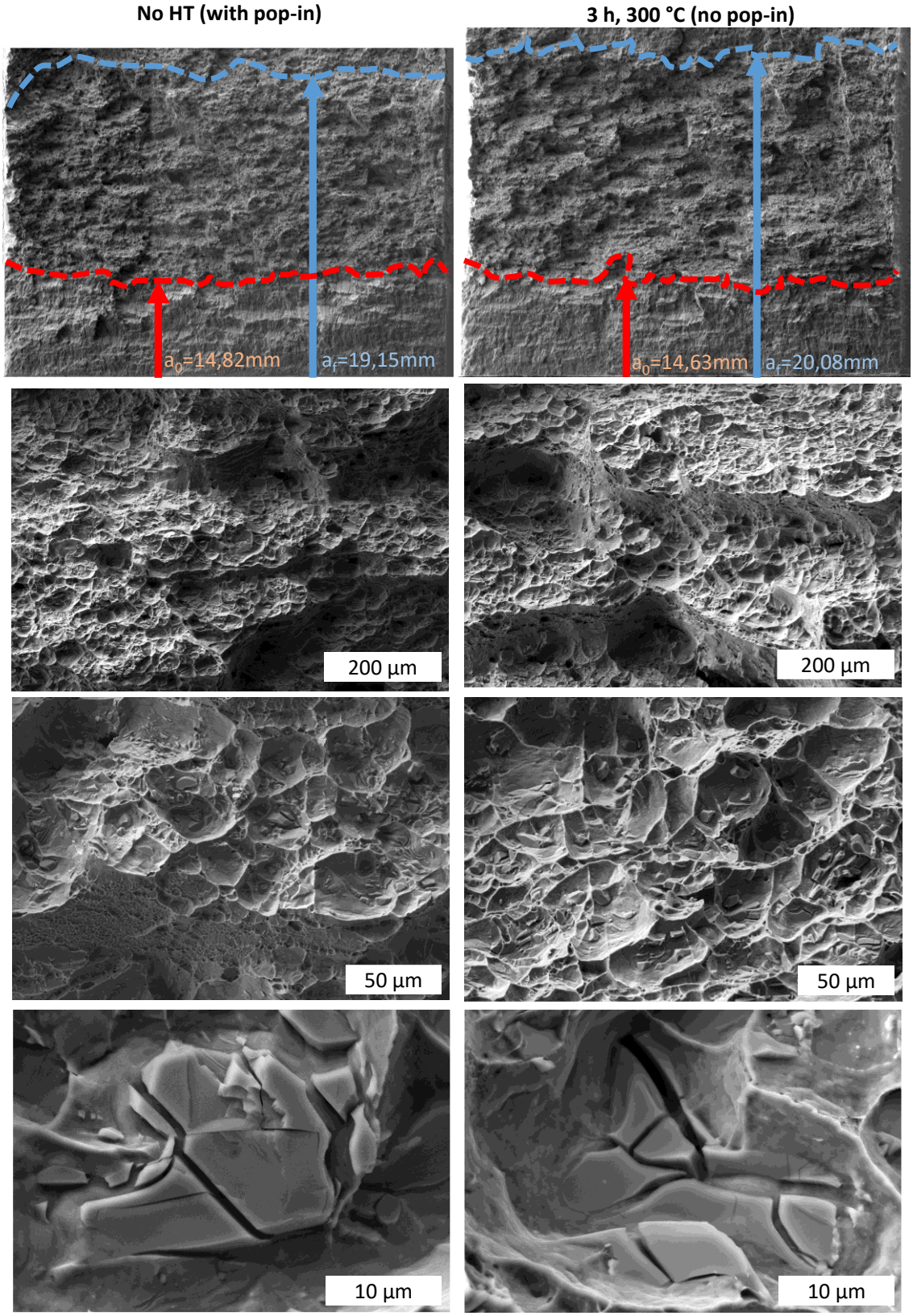

Figure 7 - Fracture surfaces (SEM fractograph) after fracture toughness tests on two irradiated CT specimens for different magnifications: with pop-in on the left (no HT), no pop-in on the right (3 h, 300°C)

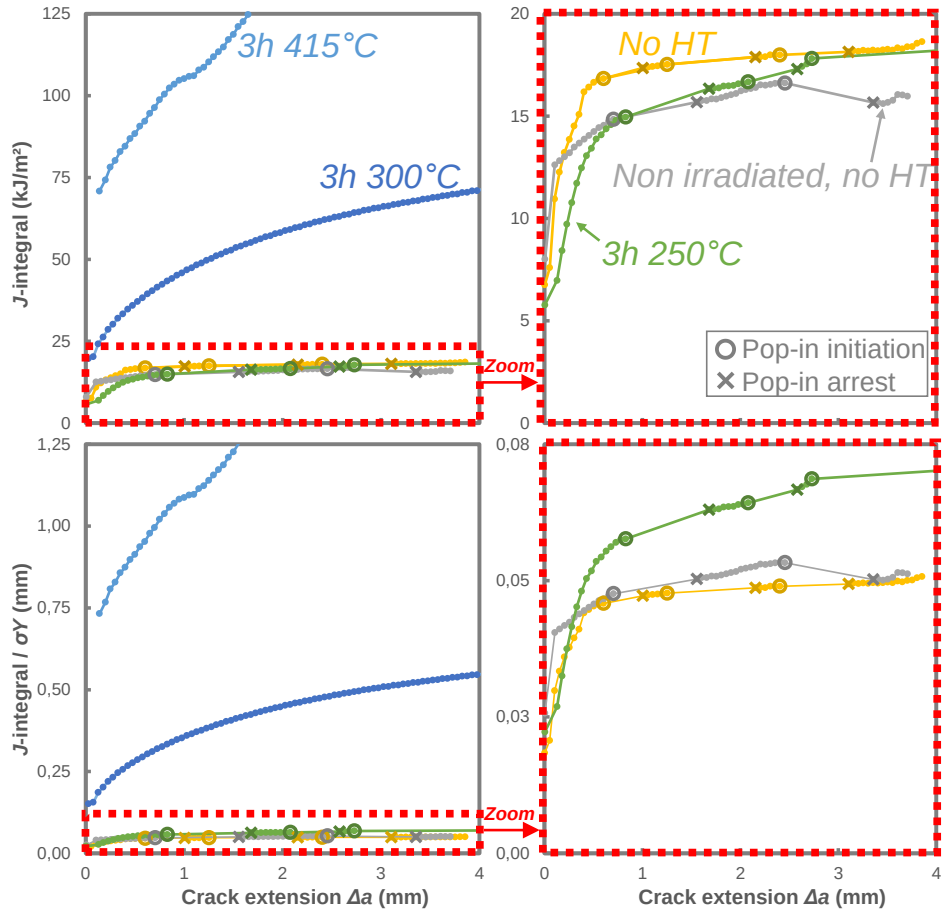

Figure 8 - Experimental J-Δa curves deduced from fracture toughness tests on unirradiated (gray, no HT) and irradiated states (the other curves, with or without HT). On the bottom curves, J values are normalized by the flow stress. The two figures on the right are a zoom of the two figures on the left.

In the calculation of J, two contributions are summed up, called the elastic part J_e and the plastic part J_p. Figure 9 shows these two contributions for two irradiated specimens:

- For the specimen without heat treatment, the elastic part is preponderant: it contributes to an average 88 % of the total J value. Despite the low contribution of plasticity, fracture is stable but for limited pop-ins as opposed to brittle fracture observed e.g. in ferritic steels. The specimen remains intact, and the fracture mechanisms are ductile as observed previously. Figure 9 allows the level of energy dissipated in the specimen to be visually quantified : it is this low energy dissipation in the plasticity that will generate the appearance of pop-in.
- For the specimen with heat treatment (3 h at 300 °C), the proportions are completely reversed: the elastic part only contributes to an average 13 % of the total J value, and the plastic part dominates (87%). It is the plasticity that controls rupture.

Table 5 gathers the crack initiation toughness $J_{0.2}$ and the material tearing modulus T_{mat} deduced from these curves. There is a slight decrease in tearing modulus with irradiation. As expected, in the irradiated state, the disappearance of pop-ins with HT is accompanied by a sharp increase in fracture toughness properties.

		Unirradiated	Irradiated			
		No HT	No HT	3 h 250 °C	3 h 300 °C	3 h 415 °C
$J_{0.2}$	kJ/m²	13.1	13.6	9.3	29.7	84.2
T_{mat}	MPa	0.96	0.6	1.4	14.7	36.2

Table 5 - Toughness parameters deduced from fracture toughness tests (Figure 8)

These results are qualitatively and quantitatively very similar to those obtained by Weeks [9] and especially Alexander [6,23]. Indeed, in Figure 10, our results comparable to the literature studies (unirradiated and irradiated specimens that have not undergone heat treatment) are added to the bibliographic data gathered in Figure 1, using the following relation [26]:

$$K_J = \sqrt{\frac{EJ_{0.2}}{1-\nu^2}} \qquad \text{Eq. 2}$$

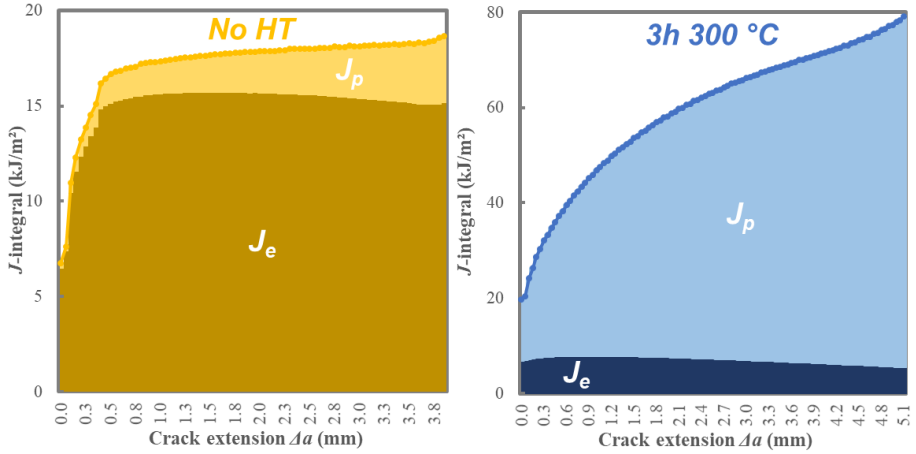

Figure 9 - Experimental J-Δa curves deduced from fracture toughness tests irradiated states (no HT and 3h at 300 °C) with the contributions of elastic and plastic parts (J_e and J_p respectively).

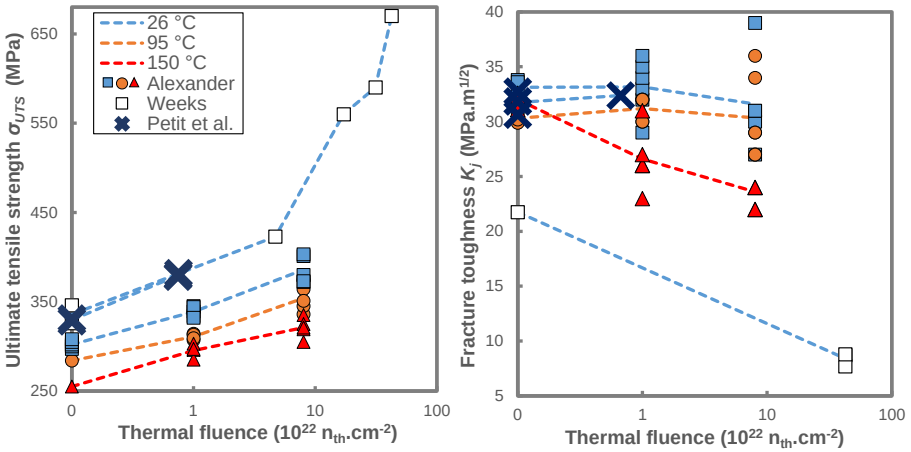

Figure 10 - Evolution of ultimate tensile strength σ_{UTS} and fracture toughness K_J in function of thermal conventional fluence for three test temperatures. Graphs using Alexander's [6,23], Petit's [the present study], Weeks' [9] data, respectively with a thermal/fast neutron fluence ratio of 2, 5 and 21.

Petit et al. [1] established two instability initiation conditions. The first one (referred to as "total displacement condition") uses the specimen total displacement u_s, the load P and the constant machine stiffness K_m:

$$\frac{dP}{du_s} \leq -K_m \qquad \text{Eq. 3}$$

Pop-in appearance using the total displacement condition can be graphically interpreted (Figure 3). A pop-in is triggered when the additive inverse of the machine stiffness (which is independent on crack length) equals to the local slope of the $P(u_s)$ curve. It is therefore shown that this pop-in type can only occur when the derivative of the curve is negative, and thus only during the unloading part of the test, i.e. after the maximum load. Crack arrest can be graphically interpreted as an intersection between the line of slope -K_m passing through the pop-in initiation point and the P-u_s curve [31].

Following the reasoning developed by Paris et al. [32], Petit et al. [1] established another criterion for the general small-scale yielding (SSY) case, using J-integral and adding the usual plastic zone correction to the crack length:

$$T_{mat} = \frac{dJ_{mat}}{da} \leq T_{app}(P, a_{eff}) \qquad \text{Eq. 4}$$

where T_{mat} is the intrinsic tearing modulus of the material and T_{app} the applied tearing modulus.

The instability criteria are applied in Figure 11. Here, the stiffness of the test machine is constant (18 kN/mm). The test without pop-in corresponds to a stable crack advance according to the criteria, while the pop-ins of the second test are correctly analysed and correspond to mechanical instabilities.

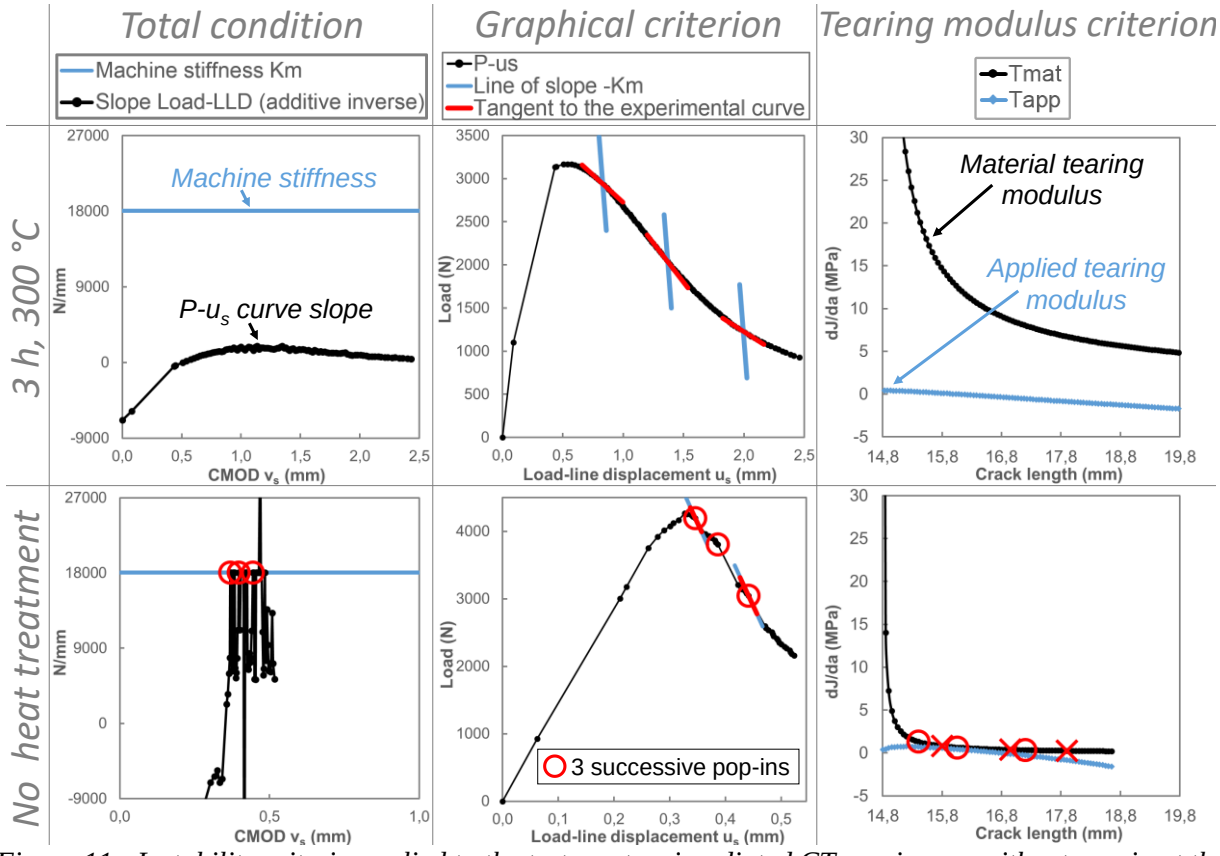

Figure 11 - Instability criteria applied to the tests on two irradiated CT specimens: without pop-in at the top (3 h, 300 °C), with pop-in on the bottom (no HT)

The pop-ins observed in the irradiated state are therefore of the same type as those occurring in the unirradiated state: they are mechanical instabilities, and they are not due to microstructural

heterogeneities. The reduction of the tearing modulus leads to a steeper load decrease during crack extension so that the system consisting of the specimen and the testing machine becomes unstable.

This reduction of the tearing modulus directly results from the hardening of the matrix, caused by the irradiation and the defects that it generates. The same explanation was proposed in [25] for the unirradiated material with various aging times, all leading to hardening. In that case ageing had the same effect than irradiation. Indeed if heat treatments lead to softening (3 h at 300 °C or 415 °C in this study), both toughness and material tearing modulus increase so that pop-ins eventually disappear.

Since the hardening has a direct effect on toughness, the insertion of a stress-driven nucleation criterion [25] seems even more relevant. In fact, the stress levels reached by hardening (regardless of its origin) appears really predominant with respect to the microstructure or the fracture mechanisms.

5. Conclusions

To study the effect of neutron irradiation on crack propagation instabilities and damage mechanisms, different states of a 6061 aluminium alloy are investigated by tensile tests, toughness tests and fractography. These conditions included the as received T6 material, the material after irradiation and conditions with more or less severe heat-treatments after irradiation that soften the irradiated material.

From a literature review, it is concluded that neutron irradiation causes the hardening of the 6061 aluminium alloy by different phenomena (damage, defects, bubbles, transmutation ...). This hardening of the matrix is fundamentally different from that caused by the aging to reach the T6 state, but it leads to the same result: a reduction of the tearing modulus.

It is shown by a stability analysis that, in interaction with the system stiffness, the decrease of tearing modulus favours mechanical instabilities, which trigger the appearance of pop-ins. These pop-ins are identified as sudden accelerations of the ductile crack advance. To investigate experimentally if the crack propagation instabilities are related to the tearing moduli, heat treatments of the irradiated material are applied that soften the material. It is shown that with softening, the number of crack propagation instabilities decreases and eventually the pop-ins disappear. The instability criteria using J-Δa R-curves of the toughness tests are applied and it is concluded that the increase in pop-ins with irradiation is resulting from the decrease of the material tearing modulus (and its interaction with the machine stiffness).

The instability phenomena are shown to not be the result of changes in the fracture mechanisms: fractographic examination reveals that regardless of the conditions (irradiated or unirradiated, with or without HT), the ductile damage mechanisms are the same. They involve nucleation, growth and coalescence of voids. Hardening has the largest influence on the decrease in toughness, probably by promoting the rupture of brittle micrometer-sized particles. Faster damage nucleation then supposedly leads to an accelerated crack extension, a decrease of the tearing modulus and consequently to pop-ins.

Acknowledgements

This work was fully funded and supported by The French Alternative Energies and Atomic Energy Commission, within the project PRT. The authors wish to thank Philippe Grange, Etienne Guillot, Johann Pegaitaz and Isabelle Turque for their contribution to the mechanical tests, Marie Azera for fractographic investigations and Bénédicte Kapusta for calculations of transmuted silicon fraction. They also acknowledged many fruitful discussions with Bénédicte Kapusta and Benoît Tanguy.

6. References

[1] T. Petit, C. Ritter, J. Besson, T.F. Morgeneyer, Impact of machine stiffness on “pop-in” crack propagation instabilities, Eng. Fract. Mech. 202 (2018) 405–422. https://doi.org/10.1016/j.engfracmech.2018.08.007.

[2] K. Buchanan, K. Colas, J. Ribis, A. Lopez, J. Garnier, Analysis of the metastable precipitates in peak-hardness aged Al-Mg-Si(-Cu) alloys with differing Si contents, Acta Mater. 132 (2017) 209–221. https://doi.org/10.1016/j.actamat.2017.04.037.

[3] A. Chbihi, S. Vincent, J. Ribis, C. Toffolon-Masclet, J. Garnier, Influence of plastic deformation on the precipitation sequence in an AA6061 alloy, J. Mater. Sci. 52 (2017) 6063–6073. https://doi.org/10.1007/s10853-017-0845-8.

[4] D. Bardel, M. Perez, D. Nelias, A. Deschamps, C.R. Hutchinson, D. Maisonnette, T. Chaise, J. Garnier, F. Bourlier, Coupled precipitation and yield strength modelling for non-isothermal treatments of a 6061 aluminium alloy, Acta Mater. 62 (2014) 129–140. https://doi.org/10.1016/j.actamat.2013.09.041.

[5] R.T. King, A. Jostsons, K. Farrell, Neutron irradiation damage in a precipitation-hardened aluminum alloy, Amer Soc Test Mater Spec Tech Publ. (1973) 165–180.

[6] D. Alexander, The effect of irradiation on the mechanical properties of 6061-T651 aluminum, Eff. Radiat. Mater. 16th Int. Symp. ASTM STP 1175 Am. Soc. Test. Mater. Phila. USA. (1993).

[7] K. Farrell, A.E. Richt, Postirradiation properties of the 6061-T6 aluminum High Flux Isotope Reactor hydraulic tube, 1976.

[8] K. Farrell, R.T. King, Tensile properties of neutron-irradiated 6061 aluminum alloy in annealed and precipitation-hardened conditions, Eff. Radiat. Struct. Mater. ASTM STP 683. (1978) 440–449.

[9] J. Weeks, C. Czaijkowski, K. Farrell, Effects of high thermal neutron fluences on type 6061 aluminum, Eff. Radiat. Mater. 16th Int. Symp. ASTM STP 1175 Am. Soc. Test. Mater. Phila. USA. (1993).

[10] C. Flament, J. Ribis, J. Garnier, Y. Serruys, F. Leprêtre, A. Gentils, C. Baumier, M. Descoins, D. Mangelinck, A. Lopez, K. Colas, K. Buchanan, P. Donnadieu, A. Deschamps, Stability of β″ nano-phases in Al-Mg-Si(-Cu) alloy under high dose ion irradiation, Acta Mater. 128 (2017) 64–76. https://doi.org/10.1016/j.actamat.2017.01.044.

[11] B. Kapusta, Estimation du gonflement du 6061-T6. Note CEA, SEMI/LCMI/NE/2008/003/A, (2008).

[12] J. Ribis, P. Donnadieu, C. Flament, J. Garnier, F. Leprêtre, Y. Serruys, A. Deschamps, Radiation-induced cavities in aluminium alloy imaged by in line electron holography, 2016. https://doi.org/10.1080/14786435.2016.1205230.

[13] A. Jostsons, R.T. King, Transmutation-produced Mg2Si precipitation in an irradiated Al-2.5% Mg alloy, Scr. Metall. 6 (1972) 447–451. https://doi.org/10.1016/0036-9748(72)90027-0.

[14] K. Farrell, J.O. Stiegler, R.E. Gehlbach, Transmutation-produced silicon precipitates in irradiated aluminum, Metallography. 3 (1970) 275–284. https://doi.org/10.1016/0026-0800(70)90015-7.

[15] K. Farrell, Performance of Aluminum in Research Reactors, Compr. Nucl. Mater. 5 (2012) 143–175. https://doi.org/10.1016/B978-0-08-056033-5.00113-0.

[16] K. Farrell, Microstructure and tensile properties of heavily irradiated 5052-0 aluminum alloy, J. Nucl. Mater. 97 (1981) 33–43. https://doi.org/10.1016/0022-3115(81)90415-3.

[17] K. Farrell, Radiation-induced strengthening of 6061-T6 Al discriminayed by thermal and fast fluence, Proceeding Mater. Res. Soc. Symp. Microstruct. Irradiat. Mater. 373 (1995) 165–170.

[18] C. Flament, J. Ribis, J. Garnier, T. Vandenberghe, J. Henry, A. Deschamps, Electron irradiation-enhanced core/shell organization of Al(Cr, Fe, Mn)Si dispersoids in Al–Mg–Si alloys, Philos. Mag. 95 (2015) 906–917. https://doi.org/10.1080/14786435.2015.1009959.

[19] B. Kapusta, C. Sainte-Catherine, X. Averty, G. Campioni, A. Ballagny, Mechanical Characteristics of 5754-Net-O Aluminum Alloy Irradiated up to High Fluences: Neutron Spectrum and Temperature

Effects. 1st Joint Meeting of the National Organization of Test, Research and Training Reactors And The International Group on Research Reactors, in: Gaithersburg, USA, 2005.
[20] A. Munitz, A. Shtechman, C. Cotler, M. Talianker, S. Dahan, Mechanical properties and microstructure of neutron irradiated cold worked Al-6063 alloy, J. Nucl. Mater. 252 (1998) 79–88. https://doi.org/10.1016/S0022-3115(97)00293-6.
[21] J. Weeks, C. Czaijkowski, P. Tichler, Effects of high thermal and high fast fluences on the mechanical properties of type 6061 aluminum in the HFBR, ASTM STP 1046. (1990) 441–452.
[22] L. Albertin, J. DeMastry, Post-Irradiation tensile and fracture toughness properties of 6061-T651 aluminium plate, Pap. Present. Symp. Eff. Radiat. Struct. Mater. Los Angel. Ca. (1972).
[23] D. Alexander, The Effects of Irradiation on the Mechanical Properties of 6061 -T651 Aluminium Base Metal and Weldments, Eff. Radiat. Mater. 16th Int. Symp. ASTM STP 1325 Am. Soc. Test. Mater. (1999) 1027–1044.
[24] T. Petit, Comprehension and modeling of toughness tests with pop-in : application to 6061-T6 aluminum and effect of neutron irradiation, Thesis, MINES Paristech, 2018. http://www.theses.fr/2018PSLEM019/document.
[25] T. Petit, J. Besson, C. Ritter, K. Colas, L. Helfen, T.F. Morgeneyer, Effect of hardening on toughness captured by stress-based damage nucleation in 6061 aluminum alloy, Acta Mater. 180 (2019) 349–365. https://doi.org/10.1016/j.actamat.2019.08.055.
[26] ASTM International, West Conshohocken (PA, USA), ed., ASTM E1820-17, Standard test method for measurement for fracture toughness, (2017).
[27] E. Voce, The relationship between stress and strain for homogeneous deformations, J. Inst. Met. 74 (1948) 537-562.
[28] K.C. Prince, J.W. Martin, The effects of dispersoids upon the micromechanisms of crack propagation in Al-Mg-Si alloys, Acta Metall. 27 (1979) 1401–1408. https://doi.org/10.1016/0001-6160(79)90209-8.
[29] G. Liu, S. Scudino, R. Li, U. Kühn, J. Sun, J. Eckert, Coupling effect of primary voids and secondary voids on the ductile fracture of heat-treatable aluminum alloys, Mech. Mater. 43 (2011) 556–566. https://doi.org/10.1016/j.mechmat.2011.06.014.
[30] Y. Shen, T.F. Morgeneyer, J. Garnier, L. Allais, L. Helfen, J. Crépin, Three-dimensional quantitative in situ study of crack initiation and propagation in AA6061 aluminum alloy sheets via synchrotron laminography and finite-element simulations, Acta Mater. 61 (2013) 2571–2582. https://doi.org/10.1016/j.actamat.2013.01.035.
[31] F. Rivalin, A. Pineau, M. Di Fant, J. Besson, Ductile tearing of pipeline-steel wide plates: I. Dynamic and quasi-static experiments, Eng. Fract. Mech. 68 (2001) 329–345. https://doi.org/10.1016/S0013-7944(00)00107-7.
[32] P.C. Paris, H. Tada, A. Zahoor, H. Ernst, The theory of instability of the tearing mode of elastic-plastic crack growth, ASTM STP Elastic-Plast. Fract. JD Landes JA Begley GA Clarke. 668 (1979) 5–36. https://doi.org/10.1520/STP35825S.

Appendix A

Calculation of the *Si* transmutation rate

Consider a cylinder made of an aluminium alloy containing a density N_{Al} of ^{27}Al aluminium atoms. The number of atoms in this cylinder is equal to SLN_{Al}, where S is the cross section of the cylinder and L its length. The resulting effective neutron capture cross section for the cylinder is then $\Sigma = SLN_{Al}\sigma$. The resulting capture probability is then: $P = \frac{\Sigma}{S} = LN_{Al}\sigma$.

The microscopic surface of a ^{27}Al nucleus as seen by an incident neutron for a given nuclear reaction is called the effective cross-section for that reaction. It is a function of the energy of the incident neutron and the temperature of the aluminium alloy. It is noted:

- N_{Al} (a/cm^3): atom density of ^{27}Al
- N_{Si} (a/cm^3): atom density of ^{28}Si
- σ (cm²): neutron capture cross section ^{27}Al (n,γ)
- ϕ_{th} (n/cm²/s): flux in conventional thermal neutrons
- P: probability of neutron capture by ^{27}Al
- V(cm^3): cylinder volume

And for a time increment dt:

$$dN_{Si} = S\phi_{th}\frac{P}{V}dt = S\phi_{th}\frac{LN_{Al}\sigma}{LS}dt = \phi_{th}N_{Al}\sigma dt$$

The number of Si moles generated is equal to the number of Al transmuted:

$$dN_{Al} = -dN_{Si}$$

Thus:

$$\frac{dN_{Al}}{dt} = -\phi_{th}N_{Al}\sigma$$

Finally:

$$N_{Al} = N_{Al,unirr}e^{-\phi_{th}\sigma t}$$

In addition $N_{Al} = N_{Al,unirr} - N_{trans}$:

$$N_{trans} = N_{Al,unirr}\left(1 - e^{-\phi_{th}\sigma t}\right)$$

In practice, a chemical composition is measured in mass %:

- $m_{\%Si,unirr}$ (%): mass of *Si* in the unirradiated alloy
- $m_{\%Si,irr}$ (%): mass of *Si* in the irradiated alloy
- $m_{\%Al,unirr}$ (%): mass of *Al* in the unirradiated alloy
- $m_{\%Al,irr}$ (%): mass of *Al* in the unirradiated alloy
- $\Delta Si_{\%mass}$ (%): excess *Si* in the alloy due to transmutation $\Delta Si_{\%mass} = m_{\%Si,irr} - m_{\%Si,unirr}$
- M_{Al} and M_{Si}: atomic mass of aluminium 27 and silicium 28

Previous equations become:

$$m_{\%Al,irr}(\phi_{th}) = m_{\%Al,unirr}e^{-\phi_{th}\sigma t}$$

$$\Delta Si_{\%mass}(\phi_{th}) = m_{\%Al,unirr}\frac{M_{Si}}{M_{Al}}\left(1 - e^{-\phi_{th}\sigma t}\right)$$

The numerical application is as follows (with $E = 0.0254\ eV$ and $T = 20\ °C$): $m_{\%Al,unirr} = 97.31$ % and $\sigma = 234.4\ mbarns = 234.4\ 10^{-27}\ cm^2$.The results are shown in the Figure 12, which illustrates the evolution of aluminium and silicon content as a function of thermal fluence. It can be seen that the rate of transmuted silicon follows a linear evolution.

The chemical composition of an initially unirradiated 6061 alloy can exceed the range of validity of mass concentrations during irradiation; indeed, using the initial chemical composition of the material in this study, the higher mass concentration limit of Si (0.8 %) is reached from 6.2 10^{21} $n_{th.conv}$.cm^{-2}, and the lower mass concentration limit of Al (95.8 %) is reached from 64.5 10^{21} $n_{th.conv}$.cm^{-2}. At the fluence studied here (6.8 10^{21} $n_{th.conv}$.cm^{-2}), the Si concentration (0.81 %) has just exceeded the higher limit.

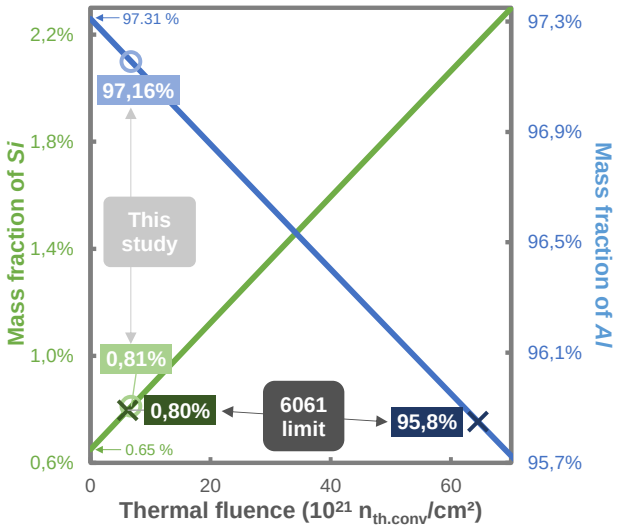

Figure 12 – Transmutation effect: evolution of aluminium and silicon content as a function of thermal fluence. The circles correspond to the fluence studied in this paper $\phi_{th} = 6.8\ 10^{21}\ n_{th.conv}/cm^2$*, and the crosses to the mass concentration limits of a 6061 alloy.*

Appendix B

EDS analysis

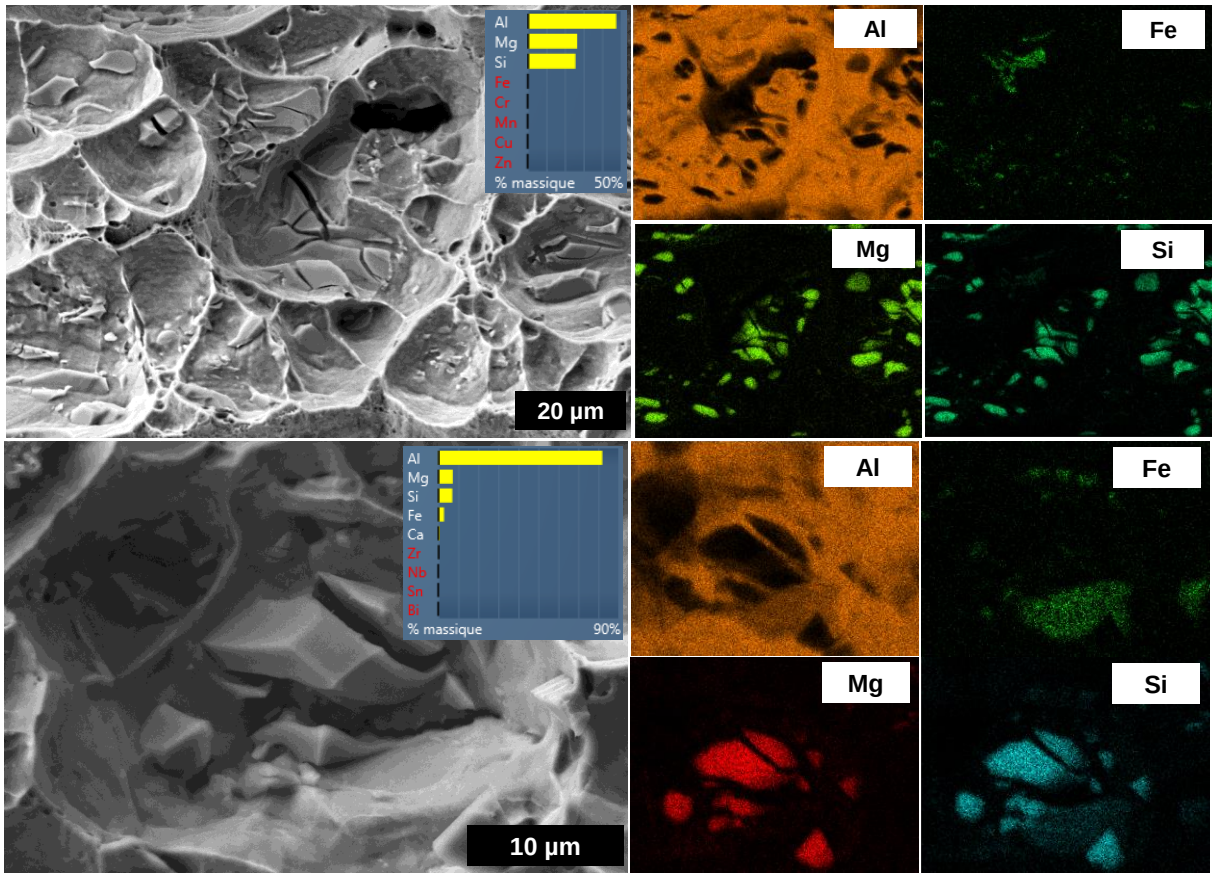

Figure 13 – Energy-dispersive X-ray spectroscopy (EDS) performed on fracture surfaces on irradiated CT specimen